Investigating RNA-RNA interactions through computational and biophysical analysis

Tyler Mrozowich[1†], Sean M. Park[1†], Maria Waldl[2,3], Amy Henrickson[1], Scott Tersteeg[1], Corey R. Nelson[1], Anneke Deklerk[1], Borries Demeler[1,4,5], Ivo L. Hofacker[2,6], Michael T. Wolfinger[2,6], Trushar R. Patel[1,7,8]*

1. Department of Chemistry and Biochemistry, Alberta RNA Research and Training Institute, University of Lethbridge, 4401 University Drive, Lethbridge, AB T1K 3M4, Canada
2. Department of Theoretical Chemistry, University of Vienna, Währinger Strasse 17, 1090, Vienna, Austria
3. Center of Anatomy & Cell Biology, Division of Cell & Developmental Biology, Medical, University of Vienna, Schwarzspanierstrasse 17, 1090, Vienna, Austria
4. Department of Chemistry and Biochemistry, University of Montana, Missoula, MT 59812, USA
5. NorthWest Biophysics Consortium, University of Lethbridge, University of Lethbridge, 4401 University Drive, Lethbridge, AB T1K 3M4, Canada
6. Bioinformatics and Computational Biology, Faculty of Computer Science, University of Vienna, Währinger Strasse 29, 1090, Vienna Austria
7. Li Ka Shing Institute of Virology, University of Alberta, Edmonton, T6G 2E1, Alberta, Canada
8. Department of Microbiology, Immunology & Infectious Diseases, Cumming School of Medicine, University of Calgary, Calgary, T2N 4N1, Canada

† These authors contributed equally to this work

*- Corresponding author email trushar.patel@uleth.ca

Supplementary Information

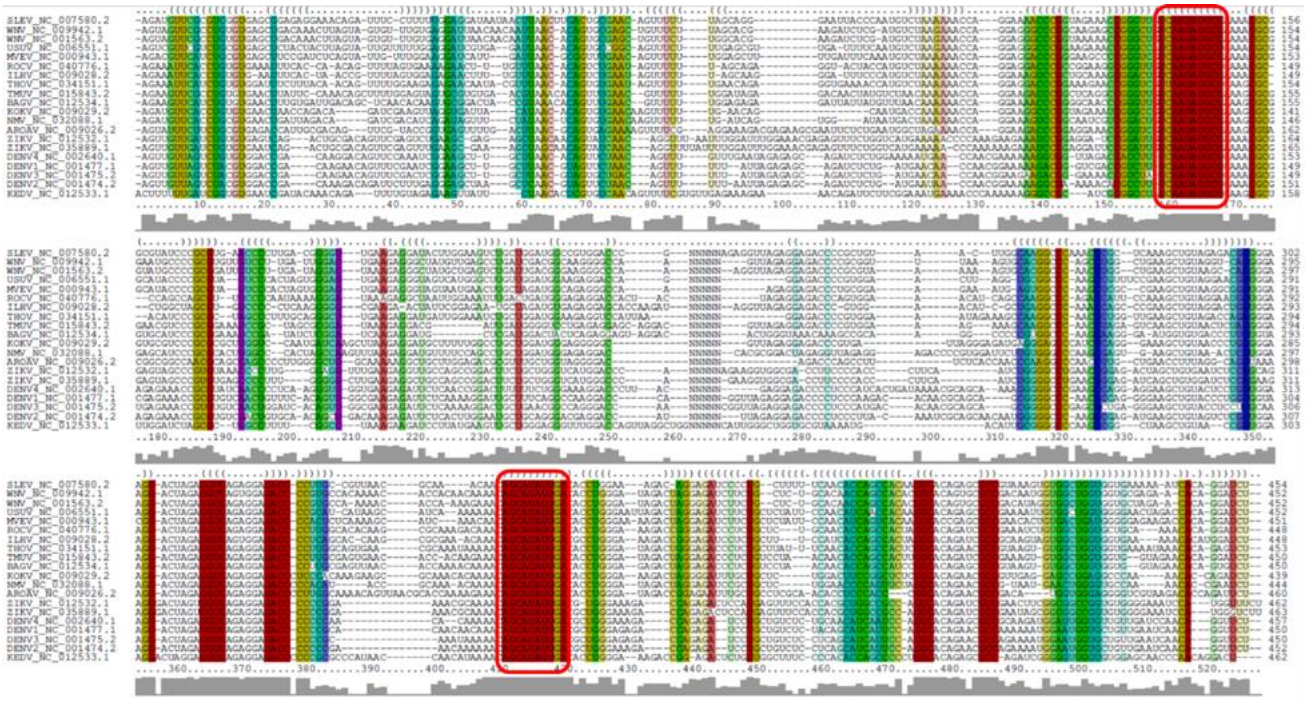

Figure S1. Multiple sequence alignment for 5'TR and 3'TR of 20 mosquito-borne Flaviviruses that was used to form the consensus structure in Fig. 2. The alignment was obtained from the structural alignment toll LocARNA, the two fragments were joined by a linker of 5 Ns. Coloring indicates covariation in consensus base pairs following the RNAalifold schema, ranging from red(no covariation, full primary sequence conservation) to violet (full covariation, all six possible combinations of base pairs). Red boxes highlight the conserved 5' and 3' cyclization sequence, respectively.

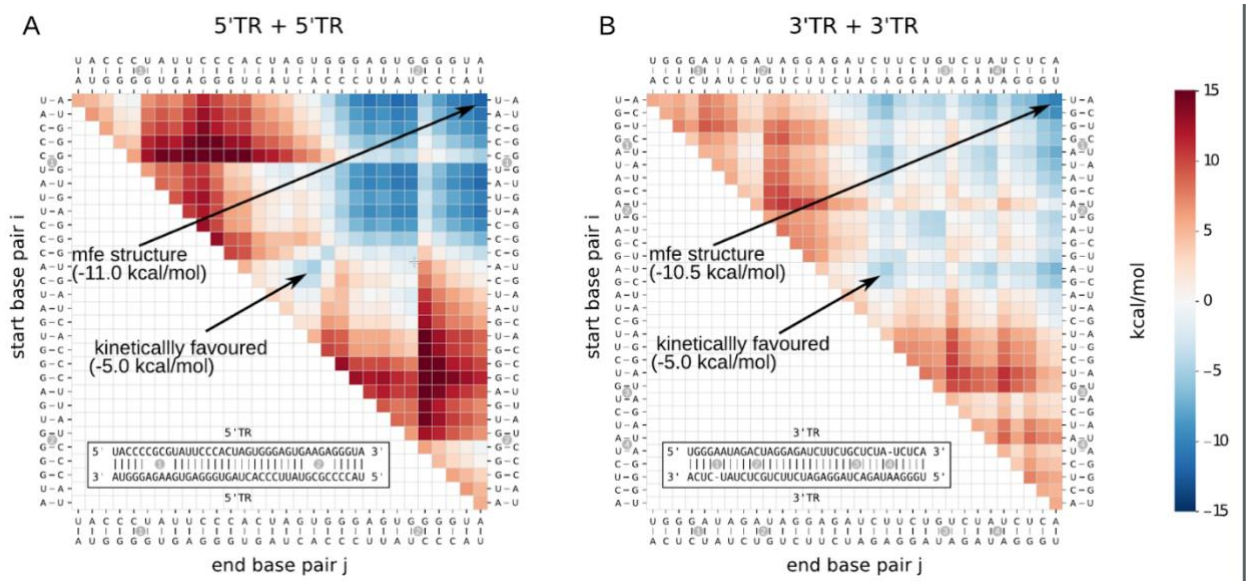

Figure S2. Energy landscapes of predicted homodimer interactions. a) 5'TR homodimer b) 3'TR homodimer. The thermodynamical model predicts stable minimum free energy structures with -11 kcal/mol and -10.5 kcal/mol, for the two respective homodimers. Based on the energy landscapes, there is no kinetically favourable path from a first base pair (drawn on the diagonal) to the full interaction (drawn in the upper right corner) through which the full interaction could be reached without crossing any energy barriers. In both examples, the most stable substructure that is energetically favourable has a stability of -5 kcal/mol and therefore is less stable than the known CS

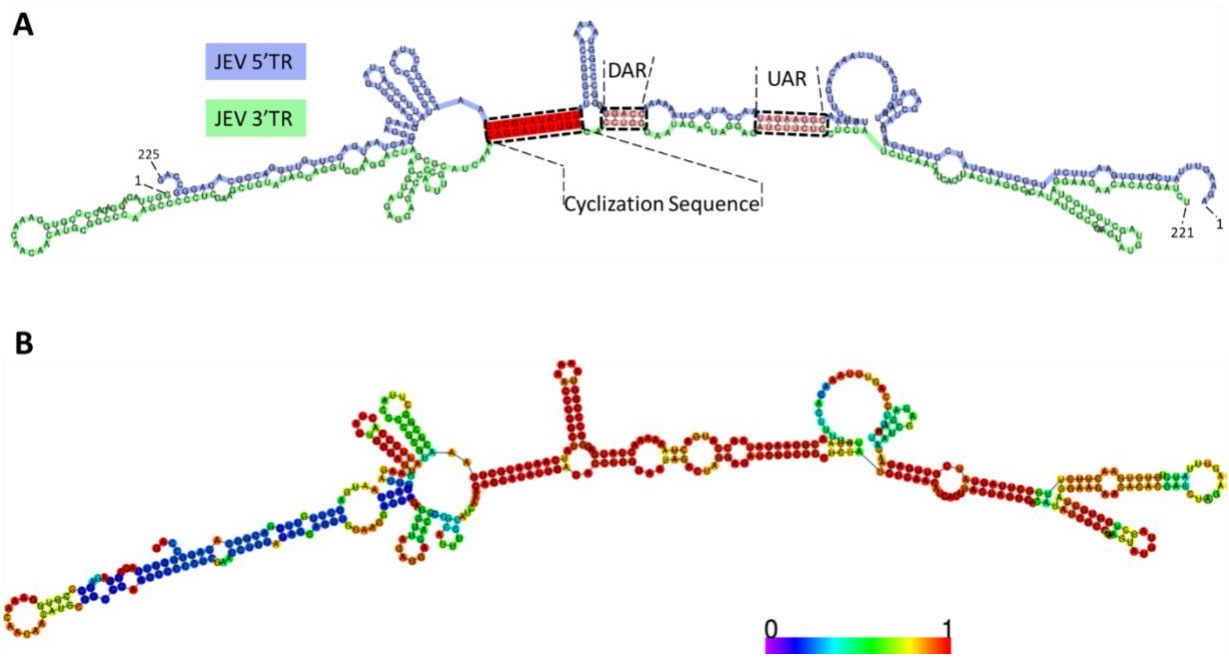

Figure S3. Predicted duplex structure of the JEV 3'TR and JEV 5'TR obtained from RNAcofold, showing the maximum possible extent of interaction. A) Known long range interaction elements, such as cyclization sequence (CS), downstream AUG region (DAR) and upstream AUG region (UAR) are highlighted; B) structure with reliability annotation (based on pair probabilities) ranging from blue (poor reliability) to red (high confidence).

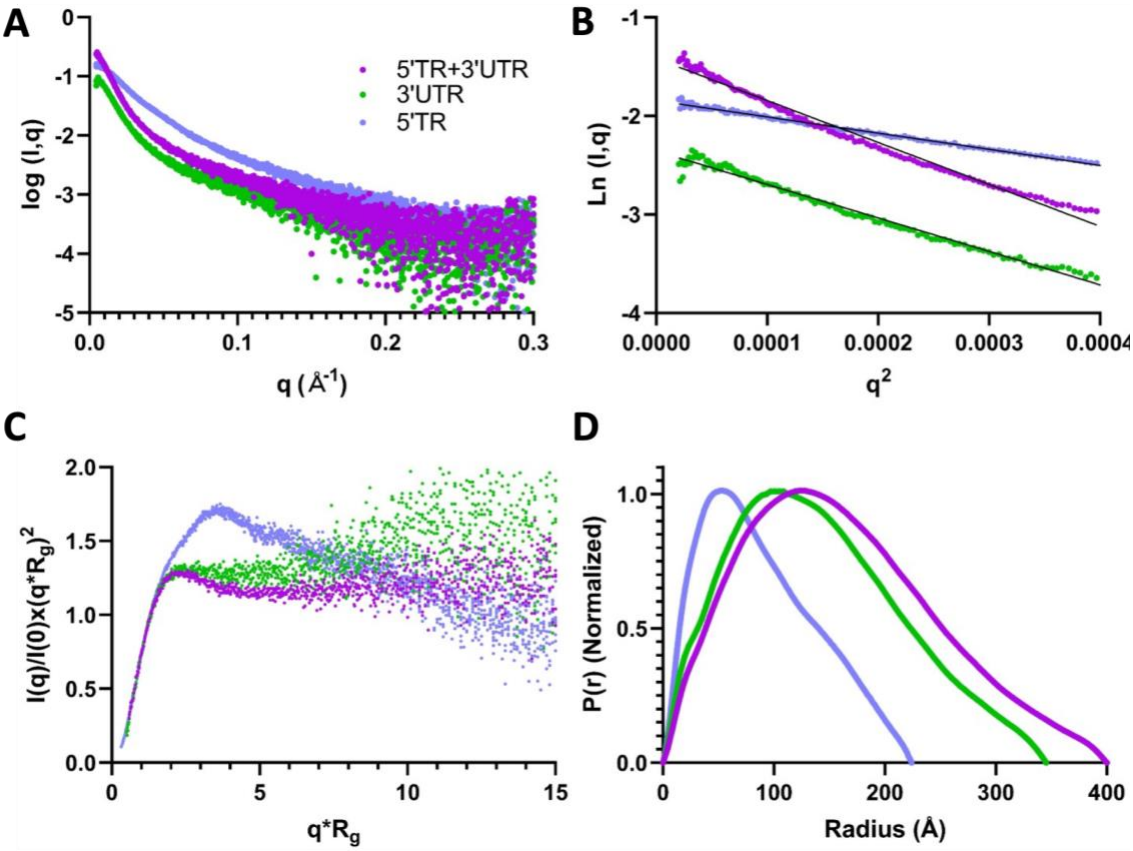

Figure S4. Small Angle X-Ray Scattering (SAXS) plots of JEV RNA-RNA interaction. A) Subtracted & merged scattering data for JEV RNA depicting the scattering intensity vs. scattering angle ($q = 4\pi\sin\Theta/\lambda$). B) Guinier plots representing the determination of R_g and homogeneity derived from the low-angle region. C) Dimensionless Kratky plots of JEV RNA depicting an elongated structure as a result of the non-Gaussian shape(s) of the curve(s). D) Pair-distance distribution plots for JEV RNA for real-space R_g and maximal particle dimension (D_{max}) determination from the entire SAXS dataset.

List of NCBI GenBank accession numbers used to analyse JEV sequences.

JN381865.1
EF623987.1
MH753131.1
MK585066.1
FJ185036.1
JN381858.1
JN381867.1
KM677246.1
AB569985.2
KF297916.1
JN381870.1
AY849939.1
KX965684.1
KF297915.1
EF107523.1
JN864064.1
AB569981.2
AB569983.2
AF221500.1
JQ086763.1
AB551990.1
MH753128.1
FJ185037.1
HM596272.1
JN381866.1
JN381863.1
AF080251.1
MH258851.1
JF706272.1
JN711459.1
JF706269.1
MH258853.1
JN381861.1
JN381873.1
JN711458.1
JN381871.1
EF571853.1
AB569990.2
MH753130.1
KF907505.1
JN381860.1
AF486638.1
KT447437.1
MH258850.1
AF315119.1
JN381864.1

MF002373.1
JN381859.1
AB569980.2
U14163.1
NC_001437.1
MF326270.1
AB569984.2
AF098737.1
EF623989.1
AF098735.1
JN381872.1
JN381869.1
AF075723.1
JN381854.1
JF706280.1
M18370.1
JF706284.1
KR265316.1
AF221499.1
AY184212.1
U47032.1
KU323483.1
AB196924.1
JX131374.1
AF416457.1
LC461960.1
EF543861.1
KP164498.2
AY508813.1
AF014160.1
MH258849.1
AF098736.1
MH258848.1
AB196925.1
MH385014.1
JN381853.1
MH753132.1
JN381856.1
JF706275.1
JF706283.1
D90194.1
KU363309.1
D90195.1
KT239164.1
AB569988.2
AF014161.1
AB569982.2
JF915894.1

JQ086762.1
JN381862.1
JN381868.1
JN381857.1
JF706273.1
HE861351.1
JN604986.1
MH258852.1
JF706285.1
AB196926.1
AB196923.1
AF069076.1
JN381855.1
JF706276.1
EF623988.1